

A method for non-invasive full-field imaging and quantification of chemical species†

Cite this: DOI: 10.1039/c3lc41293h

Viktor Shkolnikov and Juan G. Santiago*

We present a novel method for full-field scalar visualization and quantification of species concentration fields. We term this method species-altered fluorescence imaging (SAFI). The method employs electrically neutral fluorescent dyes whose quantum yields are selectively quenched or enhanced by species of interest. SAFI enables simultaneous imaging of material interfaces and provides non-invasive, scalar-field quantitation of two-dimensional species concentration fields. We describe criteria for choosing SAFI dyes and tabulate 35 promising SAFI dyes and their relevant properties. Next, we describe species concentration quantification with SAFI *via* Stern–Volmer quenching and discuss the sensitivity and resolution of our method. We demonstrate this method with two dyes, 6-methoxy-*N*-(3-sulfopropyl)quinolinium (SPQ) and 10-(3-sulfopropyl)acridinium betaine (SAB). We demonstrate our method in full-field visualization of several challenging electrokinetic flows: isotachopheresis (ITP) in both cationic and anionic modes, and in a convective electrokinetic instability (EKI) flow. Through these experiments we collectively quantify ion concentration shock velocities, simultaneously measure concentrations of five species, and quantify the development of an unsteady, chaotic, 2D flow.

Received 23rd November 2012,
Accepted 29th January 2013

DOI: 10.1039/c3lc41293h

www.rsc.org/loc

1. Introduction

The past 20 years has seen rapid growth of microfluidic and microscale chemical analysis systems.^{1,2} These systems manipulate small volumes of fluid often containing several chemical species, and create spatially and temporally varying flows and concentration fields.² Dynamic, full-field visualization and quantitation of these unsteady species concentration fields is needed for greater understanding and optimization of the underlying phenomena in these systems and for system design and validation. To this end, several scalar flow visualization and quantitation techniques have been applied.³ The simplest is full field fluorescence visualization in which a fluorescent species is seeded into a flow and tracked as a tracer to qualitatively or quantitatively analyze the flow.³ Similar to fluorescence visualization are photobleaching, phosphorescence, photochromatic reactions, and caged fluorescence techniques. In the latter four techniques, a sub-region or pattern (*e.g.*, a timeline) may be marked by exposing the sub-region to intense visible or ultraviolet (UV) radiation, locally altering the luminescence of the tracer.^{3,4} The development of the sub-region provides information regarding the flow.^{3,4} For example, in caged-fluorescence visualization,⁵ a caged molecule is mixed homogeneously in the flow, and illumination

with (typically ultra-violet laser) light breaks a chemical bond, creating a new, fluorescent species in the illuminated region. Similarly, in bleached fluorescence visualization,⁶ a fluorescent tracer is homogeneously mixed in the flow and laser light near the excitation wavelength can be used to photobleach patterns into the flow. Another luminescence-based flow visualization technique is the fluorescence quenching technique. Here luminescence of a single primary tracer is quenched when it encounters a single secondary, quenching tracer. Unlike the four techniques above, the luminescence of a sub-region is determined by the concentration of the fluorescent tracer and that of quenching species. This technique is most commonly employed to study mixing in microflows.^{7–9}

In general, luminescence based techniques offer high sensitivity and are easy to implement in microfluidic devices.^{3,10} However, such visualizations provide information associated with the concentration and quantum yield of the luminescent tracers themselves and little information concerning concentrations of other species which may be endogenous to the flow and its application. Furthermore, luminescent dye molecules chosen for these visualizations are very often electrically non-neutral, so their motion is subject to both local fluid velocity and electric fields. The latter limitation is important as the flow field may have either applied electric fields or it may generate non-negligible internal electric fields, as in the case of liquid junction potentials associated with high spatial gradients of ionic species with varying diffusivities.¹¹ These drawbacks of

Department of Mechanical Engineering, Stanford University, Stanford, CA 94305, USA. E-mail: juan.santiago@stanford.edu; Fax: +1 650-723-7657; Tel: +1 650-723-5689

† Electronic supplementary information (ESI) available. See DOI: 10.1039/c3lc41293h

charged dyes are always important for the very common case of electrokinetic microflows.

We know of only two previous techniques which address the need for full-field quantitation of endogenous, non-fluorescent ionic species in electrokinetic flows: the work of Reijenga *et al.*¹² and Chambers *et al.*¹³ Reijenga *et al.*¹² developed a method for visualizing the locations of ion concentration shocks, such as those in moving boundary electrophoresis and isotachophoresis. Reijenga *et al.* used a fluorescent dye which served as the counterion to the endogenous ions of interest in the entire flow field. In each analyte zone, the dye's concentration adjusts according to conditions of net neutrality and current conservation, and the dye's fluorescence is differentially quenched by different analytes. Dye fluorescence therefore varies across zones and can be used to identify zone interface locations.¹² The method becomes more sensitive when zone interfaces are sharper (higher electric field gradients). However, since analytes alter both the dye quantum yield and dye concentration, this creates an ambiguity in the fluorescence signal, and so it is not feasible to directly quantify absolute analyte concentration using this method.¹² For similar flows, Chambers *et al.* developed the non-focusing tracer method (NFT) which does allow for quantitation of endogenous ion concentration.¹³ The NFT method leverages migration of the fluorescent tracer in non-uniform electric fields. As the dye enters regions of low or high electric field, the dye concentration increases or decreases, respectively, in accordance with conservation of dye electrophoretic flux.¹³ The method thus allows quantification of the spatial distribution of the electric field, from which ion concentration between shocks can be calculated. The latter method requires strong gradients in electric field and *a priori* knowledge of the direction of dye flux to quantify the concentration fields. While the methods of Reijenga *et al.* and Chambers *et al.* allow for dynamic and full field visualization of ion concentration profiles, their constraints and implementation make them most suitable to one dimensional electrokinetic flows with high electric field gradients. Further, both of these methods also use ionic tracer molecules which may not be suitable for applications involving low ion density endogenous ions.

Point- or small-volume-averaging detectors are most commonly used to directly or indirectly quantify local ion concentrations in microflows. These traditionally include temperature, conductivity, electrochemical, and UV absorbance detectors.^{14–16} Small-volume-averaging detection schemes have also been based on fluorescence quenching of electrically neutral dyes. For example, quenching of an electrically neutral dye has been used to estimate biological intercellular chloride values as a function of time¹⁷ and to monitor chloride transport across cell membranes¹⁸ and vesicle membranes.¹⁷ However, the latter applications of fluorescence quenching of electrically neutral dyes are essentially monitoring of local ion concentrations in some discrete volume such as a cell or vesicle. Obviously, local or volume-averaging detections of ion concentrations are insuffi-

cient in analyzing spatially and temporally evolving scalar fields associated with many fluid flows.

We here present a novel method we term species-altered fluorescence imaging (SAFI) to address the need for full-field quantitation of endogenous, non-fluorescent species concentrations in microflows. The method is especially useful for flows with some electrokinetic component, but is generally applicable to monitoring spatial and temporal variations of species concentration fields. SAFI employs electrically neutral fluorescent dyes, whose quantum yield is selectively enhanced or quenched by species present in solution. SAFI enables simultaneous imaging of material interfaces (between dyed and un-dyed regions) and provides a non-invasive scalar field quantitation of two-dimensional density fields of multiple endogenous chemical species. We here describe criteria for selection of SAFI dyes, provide a brief library of potential dyes, and describe the aspects of quantitation using SAFI, including method sensitivity and resolution. We then demonstrate the method, using two SAFI dyes, in the full-field visualization and quantitation of two challenging electrokinetic flows: isotachophoresis (ITP) in both anionic and cationic modes and in a convective electrokinetic instability (EKI) flow. We note that SAFI is applicable for visualizing and quantitation of a wide range of microflows.

2. Theory and concept

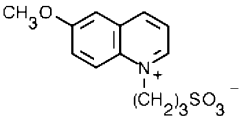
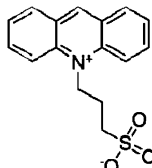
2.1 Choice of SAFI dyes

For visualizing electrokinetic flows we select SAFI dyes according to the following criteria: (a) dye is net neutral at and near the pH of interest; (b) dye exhibits negligible reactivity, complexation, or interference with species of interest or the surfaces of the fluidic system; (c) dye has a high initial quantum yield and high solubility in the solvent and at pH of interest; (d) dye fluorescence is strongly quenched or enhanced by species of interest. According to this criteria we selected and tested two dyes: 6-methoxy-*N*-(3-sulfopropyl)quinolinium (SPQ) and 10-(3-sulfopropyl)acridinium betaine (SAB). These UV excited dyes have high quantum yields and remain net electrically neutral between pH 0–12. We list a few pertinent properties for these dyes in Table 1. In sections 4.1 through 4.3 we will demonstrate visualization and quantitation of ITP and EKI using these dyes.

We have also performed a survey of other commercially available dyes that appear to fit our criteria, and selected and list 14 of these in Table 2 along with their excitation and emission wavelengths, pK_a , aqueous solubility, and molecular structure. Five of these are electrically neutral between pH 0 and 12. Nine of these dyes have no pK_a between pH 3 and 12 (as calculated with Advanced Chemistry Development Software, ACDS, V11.02²²). The latter nine dyes are excited by UV or blue light and emit in blue or green wavelengths. We also list five additional dyes with pK_a 's above 3, but which remain neutral over a sufficiently wide pH range.

In addition to the dyes shown in Table 2, we also selected 19 net electrically neutral dyes which are similar to SPQ and SAB

Table 1 Properties of SPQ and SAB SAFI dyes

Dye	SPQ ^a	SAB ^b
Working pH	0–12	0–12
Peak excitation (nm)	344	415
Peak emission (nm)	443	488
Solubility ^c	900 mM	7 mM
Relative intensity ^{c,d}	1	1.61
Molecular structure		

^a Excitation, emission, and molecular structure data from Invitrogen catalog.¹⁹ ^b Excitation, emission, and molecular structure data from Sigma-Aldrich catalog.²⁰ ^c Solubility and relative intensity data from Krapf *et al.*²¹ ^d Relative to SPQ for 0.1 mM dye concentrations; SPQ nominal quantum yield is 0.55.¹⁷

and fit our criteria for a SAFI dye, but unfortunately are not currently commercially available. These dyes were synthesized and studied by Krapf *et al.*²¹ and Huber *et al.*²³ We list these dyes and their maximum excitation and emission wavelengths, their solubility, their relative intensity, and quenching constants for chloride, bromide, and iodide in Table S1 (ESI†, Section 1). The dyes in the latter group are excited by UV or blue light and emit in blue or green wavelengths. ACDS predictions suggest these dyes remain electrically neutral between pH 0 and 12.²² Furthermore, Krapf *et al.* and Huber *et al.* have demonstrated that these dyes have excellent solubility and high quantum yield.^{21,23} In addition, chloride, bromide, iodide and other anions significantly quench these dyes' quantum yield and this quenching varies significantly among different species. We thus hypothesize that like SPQ and SAB, these dyes' quantum yield is also quenched by many other species not explored by Krapf *et al.* and Huber *et al.* We thus believe these dyes are likely useful for flow quantitation using SAFI.

2.2 Species concentration quantitation using SAFI

To quantify species concentration using SAFI we rely primarily on analyte–dye pairs exhibiting Stern–Volmer (collisional) quenching by endogenous analytes, as this provides a simple, calibration-friendly relation between analyte concentration and dye fluorescence. However, we note that analyte–dye pairs may exhibit other quenching behaviors such as static quenching, combined dynamic–static quenching and FRET, as well as fluorescence enhancement.²⁵ Furthermore, dye fluorescence intensity may appear quenched due to absorbance of light at the excitation or emission wavelength by analytes or dye (if these are in sufficiently high concentration). While we find these non-Stern–Volmer effects less useful for species concentration quantitation, we note that they can be very useful for qualitative estimates, to identify certain species, and to quantify their spatiotemporal development. For example, we discuss visualization and spatiotemporal quantitation of cationic and anionic ITP using fluorescence enhancement in

Sections 4.1 and 4.2. For quantitative applications of SAFI we shall here consider only Stern–Volmer type quenching behavior.

Here we derive the relationship between analyte concentration and change in dye fluorescence intensity for Stern–Volmer type quenching. When a fluorescent dye molecule absorbs a photon, an electron is promoted to an excited state. In Stern–Volmer type quenching, the dye molecule can lose this energy as heat, release a lower energy photon (fluorescence), or donate this energy to a quenching species *via* molecular collisions. For sufficiently low dye concentrations (and sufficiently low optical path lengths²⁶), we can assume the rate of photon energy absorbed by the dye is proportional to dye concentration.²⁵ The rate of energy released as heat or as fluorescence is also proportional to dye concentration. The rate of energy transferred to a quencher is proportional to the product of quencher concentration and dye concentration. At steady state, the rate of photon absorption by the dye is equal to the energy loss by the dye as heat, fluorescence, and collisional quenching.²⁷ Thus, following the derivation of Valeur²⁷ we can estimate the ratio of dye fluorescence intensity in absence (F_0) to that in presence (F) of quencher as

$$\frac{F_0}{F} = 1 + \left(\frac{k_{q,1}}{k_e + k_d} \right) c_1 + \left(\frac{k_{q,2}}{k_e + k_d} \right) c_2 + \dots + \left(\frac{k_{q,n}}{k_e + k_d} \right) c_n \quad (1)$$

where k_e and k_d are the proportionality constants which describe respectively the rates of dye fluorescence and of energy release as heat. Each particular k_q is the proportionality constant in the rate of energy transfer to each particular quencher i of concentration c_i (the subscript number refers to quencher species). Each term $k_{q,i}/(k_e + k_d)$ may be written as a single measurable constant $K_{Q,i}$ for each quencher:

$$\frac{F_0}{F} = 1 + K_{Q,1}c_1 + K_{Q,2}c_2 + \dots + K_{Q,n}c_n \quad (2)$$

Eqn (2) is known as the Stern–Volmer equation.²⁷ This equation implies that general quantification of each of the components of a solution with n (endogenous) quenching species requires at least n independently quantifiable SAFI dyes (each SAFI dye will have an associated Stern–Volmer equation and F_0/F measurement). We would also need to calibrate the n quenching constants for each of the n dyes, yielding n^n quenching constants. Employing additional dyes would lead to an overdetermined system of equations. The resulting equations could be solved, for example, using a least squares method, potentially reducing uncertainty in analyte concentrations.²⁸ We also note that significantly fewer dyes and quenching constants are needed to quantify the concentrations of all species in solution when some information about the composition of the solution is known *a priori*. As an example, we discuss below quantification of a solution where the relative ratios of the quenching species are expected to remain invariant. In ESI† Section 2 we provide more examples of these special cases, including quantifying a solution consisting of a single acid and a single base; and quantifying a solution with a set of analytes whose concentrations remain

Table 2 Commercially available dyes which are likely good candidates for SAFI flow field visualization and quantitation^{a,b}

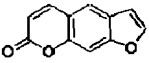
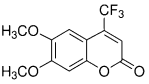
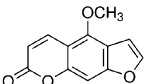
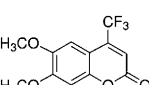
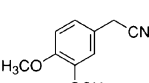
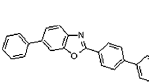
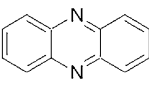
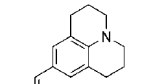
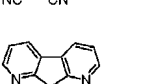
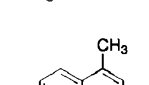
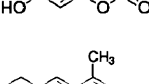
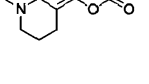
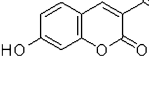
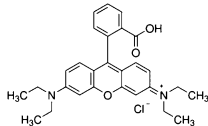
Dye	λ_{ex} (nm)	λ_{em} (nm)	Reported at	pK _a	Aq. sol. (μM)	Molecular structure
Psoralen	335	460	pH 7.0	$\ll 0$	16 000	
Dibromobimane	393	477	pH 7.0	$\ll 0$ Base	15 000	
5-Methoxypsoralen	352	480	—	$\ll 0$ Base	1100	
6,7-Dimethoxy-4-(trifluoromethyl)coumarin	358	490	DMSO	$\ll 0$ Base	2600	
(3,4-Dimethoxyphenyl)acetonitrile	430	511	pH 7.1	$\ll 0$ Base	15 000	
2-(4-Biphenyl)-6-phenylbenzoxazole	—	425	H ₂ O	1.1 Base	2100	
Phenazine	426	471	Ethyl acetate	1.60 Base	610	
9-(2,2-Dicyanovinyl)julolidine	433	500	pH 8.0; 40% glycerol	2.4 Base	290	
1,8-Diazafluoren-9-one	470	570	—	0.7 Base	2400	
4-Methylumbelliferone	372	445	—	8.0 Acid	11 000	
Coumarin 102	390	466	Ethanol	5.6 Base	130	
3-Phenylumbelliferone	338	463	pH 3.0	7.8 Acid	570	
Coumarin 153	422	532	Ethanol	5.2 Base	2	

Table 2 (Continued)

Dye	λ_{ex} (nm)	λ_{em} (nm)	Reported at	pK _a	Aq. sol. (μM)	Molecular structure
Rhodamine B	553	677	Methanol	3.2 Base ^{23,24}	—	

^a Excitation and emission data and molecular structure obtained from Sigma-Aldrich catalog.^{20 b} Solubility and pK_a data calculated *via* ACD/Labs Software V11.02²² unless otherwise noted.

invariant and a set of analytes whose relative ratios are expected to remain invariant.

In the case (Case 1) where the relative ratios of the quenching species are expected to remain invariant, we can greatly reduce the number of dyes and simplify the calibration process to quantify the concentration species present in solution. This case occurs in situations where the solution is simply diluted or concentrated, and non-idealities resulting from changes in ionic strength can be ignored (*e.g.*, activity coefficients are assumed to be unity). Here we can write the Stern–Volmer eqn (2) in terms of concentration of a single particular component of the solution and an effective quenching constant $K_{\text{Q,e}}$ for the mixture:

$$\frac{F_0}{F} = 1 + K_{\text{Q,e}}c_1 \quad (3)$$

This special case allows us to measure only a single quenching constant, for a solution containing n species, rather than n^n quenching constants as in the general case. For example, we are interested in quantifying concentration fields of varying concentrations of a solution of acetic acid and Tris and there is a constant ratio of total acetic acid to total Tris concentration (*e.g.*, two streams of varying concentration of a Tris–acetate buffer meet at an intersection). Here we require only a single calibration curve for a single value of $K_{\text{Q,e}}$ to quantify each species throughout the field.

Another special case, Case 2, is a subcase of Case 1. Here, we consider two zones, (*e.g.*, two regions in space within the same field of view of a camera). One zone, the reference zone, has known species concentrations, and the other has an unknown concentration of species. However, as required by Case 1, the unknown zone contains analyte concentration ratios which are uniform and constant. This occurs, for example, if the second zone consists of a mixing of multiple concentrations of the same buffer. We further simplify this case by assuming the SAFI dye concentrations in each zone are the same (and hence have equal values of F_0). We use the fluorescence signal of the reference zone to measure the concentration in the unknown zone. To this end, we apply eqn (3) above to each zone. Combining the respective version of eqn (3) in each zone, we obtain the following relation:

$$c_2 = \frac{1}{K_{\text{Q,e},2}} \left[\frac{F_1}{F_2} (1 + K_{\text{Q,e},1}c_1) - 1 \right] \quad (4)$$

where the subscripts 1 and 2 refer to the reference zone and the unknown zone respectively. We use Case 2 to quantify analyte concentrations in ITP experiments in Sections 4.1 and 4.2.

In the ESI,[†] we describe an additional example special case (Case 3) which simplifies calibration of and measurement using quenching dyes. Case 3 deals with a single zone (a single region in space) which contains two sets of species. One set has fixed concentrations and the second set has fixed ratios of concentrations.

2.3 Method sensitivity for Stern–Volmer quenching

We here propose a formulation to estimate the sensitivity of quantifying quencher concentrations under SAFI visualization. For the special case above, where a solution containing multiple quenching species is being diluted or concentrated, we define the sensitivity as the partial derivative of fluorescence intensity with concentration. Taking this derivative of eqn (3) we obtain

$$\frac{\partial F}{\partial c_1} = \frac{-F_0 K_{\text{Q,e}}}{(1 + K_{\text{Q,e}}c_1)^2} \quad (5)$$

We observe that this sensitivity $\partial F/\partial c_1$ is always proportional to dye fluorescence intensity in absence of quenchers, F_0 , and thus proportional to the concentration of dye and excitation illumination intensity. Additionally, for the case where the product $K_{\text{Q,e}}c_1$ is sufficiently greater than unity (*e.g.*, for 100 mM sodium chloride and SPQ dye, $K_{\text{Q,e}}c_1 \approx 10^{29}$), we see the sensitivity $\partial F/\partial c_1$ scales as $-F_0/K_{\text{Q,e}}c_1^2$. On the other hand, for the case where $K_{\text{Q,e}}c_1$ is substantially lower than unity, the sensitivity scales as the effective quenching constant, $K_{\text{Q,e}}$. Thus, when measuring low analyte concentration, the analyte–dye pair should possess a high quenching constant. Conversely, when measuring high analyte concentration, the analyte–dye pair should possess a lower quenching constant.

3. Experiments

3.1 Materials and instrumentation

SPQ and SAB were obtained from Santa Cruz Biotechnology (Santa Cruz, CA). All solutions were prepared in deionized ultrafiltered water (Fischer Scientific, Pittsburgh, PA). All other

chemicals were obtained from Sigma-Aldrich (St. Louis, MO). In isotachopheresis experiments, we suppressed electroosmotic flow with 1.3 MDa poly(vinylpyrrolidone) (PVP) from Acros Organics, (Pittsburgh, PA).

We performed both ITP and EKI experiments using commercially available, off-the-shelf optical white soda lime glass microfluidic chips (model NS12AZ, Caliper Life Sciences, Mountain View, CA). The chip channel network is a simple cross geometry and channels are wet-etched to a 20 μm depth with a 50 μm mask width; the main channel is 72 mm long (see schematic in Fig. 1). We performed the ITP experiments in galvanostatic mode with a Keithley 2410 high voltage sourcemeter (Keithley Instruments, Cleveland, Ohio). We performed the EKI experiments in potentiostatic mode with a computer-controlled Labsmith HVS-3000D high voltage sequencer (Livermore, CA).

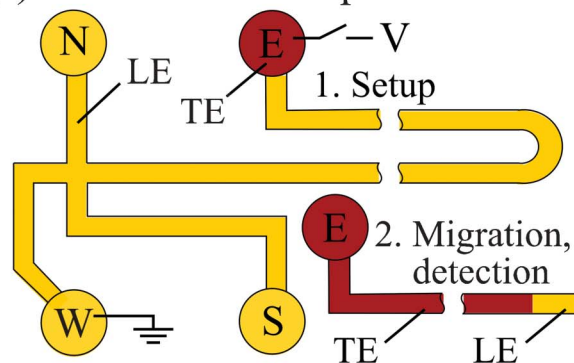
We monitored the ITP and EKI experiments with an Olympus IX70 inverted fluorescence microscope equipped with 10 \times (NA of 0.40) and 40 \times (NA of 0.60) objectives (Olympus, Hauppauge, NY), a model XF129-2 filter cube (Omega Optical, Brattleboro, VT), and 365 nm UV LED (ThorLabs Newton, NJ) for illumination. In ITP experiments, we captured images with a 12-bit 1300 by 1030 pixel charge-coupled device (CCD) camera with 6.7 \times 6.7 μm pixels (MicroMax RTE/CCD-1300Y/HS); controlled with WinView software, both from Roper Scientific (Trenton, NJ). In EKI experiments we captured images with Phantom Miro 4 M, 12-bit 600 by 800 pixel (22 \times 22 μm pixels) CMOS camera controlled with Phantom software (Vision Research, Wayne, NJ). We post-processed the images with custom in-house scripts written in MATLAB (R2010b, Mathworks, Natick, MA).

3.2 Assay protocols

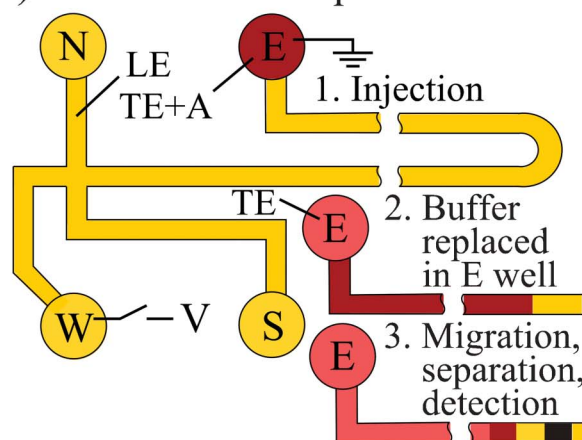
3.2.1 Measurement of effective quenching constants. We performed preliminary calibration experiments to quantify quenching constants for our buffer solutions using multiwell plates and the microscope setup described above. To this end, we placed buffers containing 5, 10, 20, 40, and 80 mM analyte in wells of a Falcon 96 well polystyrene flat bottom plate (Becton Dickinson, Franklin Lakes, NJ). We included control cases of a well which contained dye but with no analytes (to provide F_0 value) and a second well which contained pure deionized water (to provide a background value). We quantified the fluorescence in each using the CCD camera described above. To obtain the quenching constants we fit the fluorescence data to the Stern–Volmer equation (see eqn (3) Section 2.2). We provide additional recommendations regarding measuring effective quenching constants in ESI† Section 5.

3.2.2 Isotachopheresis. ITP is an electrokinetic technique used to preconcentrate and separate analytes, as well as to dilute and remove contaminants. In this technique ions form a contiguous train of discrete zones between a high electrophoretic mobility LE and low electrophoretic mobility TE ions. All ions in this train migrate at the same velocity. The zones are typically separated by self sharpening boundaries, which can be described as ion concentration shock fronts. The maximum concentrations of analyte zones are determined by the governing laws of electrophoretic migration, bulk charge

(a) Cationic isotachopheresis



(b) Anionic isotachopheresis



(c) Electrokinetic instability

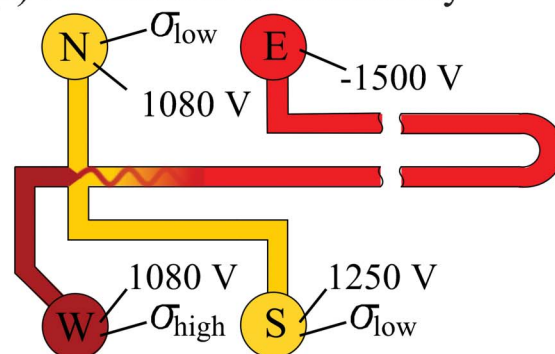


Fig. 1 Schematic of NS12AZ microfluidic chip and assay protocols for cationic and anionic isotachopheresis (ITP) and electrokinetic instability (EKI) experiments. For cationic ITP experiments (a) we filled the channel and north, south, and west wells with leading electrolyte (LE) and placed the trailing electrolyte (TE) in the east well (step 1). We then applied a constant current between the east and west wells (step 2). For anionic ITP experiments (b) we filled the channel and north, south, and west wells with LE and placed TE and analytes in the east well and applied a constant current (step 1). When the LE–analyte interface reached a fiducial marker we turned off the current and replaced the buffer in the east well with pure TE (step 2). We then applied a constant current between the east and west wells (step 3). For the EKI experiment (c) we filled the north and south wells with low conductivity electrolyte and the west well with high conductivity electrolyte; we then applied constant voltages as shown.

neutrality of the zones, and acid–base equilibrium.¹⁴ Garcia-Schwarz *et al.*³⁰ provide an introduction to ITP and a video describing its physics and example applications; the technique is thoroughly reviewed by Everaerts *et al.*¹⁴ and Bocek *et al.*³¹

We performed ITP experiments in a simple cross geometry NS12AZ caliper chip (see Fig. 1). For cationic ITP experiments we filled the channel and north, south, and west wells with leading electrolyte (LE) and placed the trailing electrolyte (TE) in the east well. We applied a constant current between the east and west wells as shown in Fig. 1. For anionic ITP experiments, we filled the channel and north, south, and west wells with LE and placed TE and analytes in the east well. We then applied a constant current, and allowed the interface between the LE and the first analyte to reach a fiducial marker (in a region approximately 5 mm from the east well reservoir). We then turned off the current and filled the west well with pure TE (no analyte). This is known as finite injection of sample in ITP. We again applied constant current, and after roughly 20 s captured images of ITP zones. For details see ESI† Section 3. We compared the experimentally observed ITP with that simulated in the generalized electrokinetics solver SPRESSO (an open-source, experimentally validated^{32–35} MATLAB-based program applicable to non-linear electrophoresis problems including ITP^{36,37}).

3.2.3 Electrokinetic instability. Electrokinetic instabilities (EKIs) are a type of electrohydrodynamic instability where microscale effects (most notably diffusion and electroosmotic flow) are important.^{38,39} These flow instabilities may arise in a wide range of electrokinetic flows which have strong gradients in electrical properties (particularly conductivity gradients) such as field amplified sample stacking, in ITP,⁴⁰ and in the analysis of multiple sample streams with poorly specified conductivities. EKI phenomena are associated with high electric fields, high conductivity gradients, and larger geometries,⁴¹ and so may limit resolution or sensitivity of a wide range of electrokinetic assays. The phenomena is also applicable to rapid low-Reynolds number mixing.⁴² EKIs occur when destabilizing electric body forces are not sufficiently damped by molecular diffusion of conductivity gradients and the viscous stresses of fluid flow. These destabilizing forces arise from a coupling of conductivity gradients and electric fields (leading to electric body forces).

We performed electrokinetic instability^{41,42} experiments also in the cross-geometry NS12AZ caliper chip. We filled the north and south wells with low conductivity electrolyte and the west well with high conductivity electrolyte; we then applied vacuum to the east well to fill the chip. We then removed vacuum and applied a constant voltage to all the wells such that an electrokinetic flow focusing develops and becomes unstable (see Fig. 1c). We then obtained images at a rate of 100 frames per second and net magnification of 25.2 (40× objective and a 0.63 demagnification lens).

4. Results and discussion

4.1 Analyte quantitation in cationic isotachopheresis

In this section, we present examples of the application of our calibrated dyes and the SAFI technique to visualize and

quantify spatiotemporal development of ion concentration fields in flows with a single sharp gradient in ion concentration (in cationic ITP). Traditionally the spatiotemporal development of ITP zones containing non-fluorescent analytes has been visualized by either the fluorescent quenching counter ion technique¹² or non-focusing fluorescent tracer technique.¹³ As mentioned above, the disadvantages of fluorescent quenching counter ion technique include the requirements that the fluorophore be an ion that is a counter-ion to the ionic species of interest and which also has a useful pK_a and is easily quenched by analytes studied.¹² On the other hand, the non-focusing fluorescent tracer technique relies on gradients in zone conductivities. Thus its disadvantage is that it may not be highly sensitive when differences in zone conductivities are small. Our SAFI technique avoids these disadvantages as it uses a neutral species, does not require selection of special counterionic species, and is able to distinguish between zones of nearly equal conductivity (due to differences in quenching constants).

We first demonstrate SAFI quantification of endogenous ions in a single interface ITP experiment. The ion concentration field values and the zone interface velocities in these flows can be compared with theoretical predictions obtained using the SPRESSO^{36,37} simulation tool. To quantify analyte concentrations in this experiment we use the approach of Case 2, Section 2.2. Here the LE zone serves as the reference zone. For simplicity, we used ITP theory to assume an expected anion-to-cation concentration ratio in the TE zone and then used the Case 2 approach to quantify the absolute concentration values. We then compared these measured absolute concentration measurements to those predicted by ITP theory. In ITP, anion-to-cation concentration ratios in individual zones trailing the LE are approximately constant in the cases where the co-ions (same sign as the leading ion) are strongly ionized and where ion effective mobility is weakly dependent on ionic strength.¹⁴ We performed our SAFI dye calibration of the endogenous TE anion and cation at the expected concentration ratio and absolute concentrations varying from 5 to 80 mM. We then measured the LE-to-TE fluorescence intensity ratio for each ITP experiment and used eqn (4) to obtain a measurement of the absolute ion concentrations in the TE. We compared these concentration values and the observed ion concentration shock speeds to those predicted theoretically with SPRESSO.^{36,37}

We then measured the quenching constant of each buffer for this characteristic anion-to-cation ratio using the method described in Section 3.2.1 by fitting the ratio of fluorescence of SPQ in the absence and presence of quencher for analyte concentrations from 5 to 80 mM to eqn (3). We plot the ratio of fluorescence of SPQ in the absence and presence of quencher at concentrations from 5 to 80 mM for pyridine–HEPES (pH 6.2), imidazole–HEPES (pH 7.1), Tris–HEPES (pH 7.3), ammediol–HEPES (pH 7.4), and sodium–HEPES (pH 7.4) buffers in Fig. 2. For SPQ dye, the fluorescence closely fit the Stern–Volmer equation (eqn (3), $R^2 > 0.99$). This indicates that these SAFI dye/buffer pairs likely exhibit Stern–Volmer type quenching. We leveraged Stern–Volmer type quenching of SPQ to quantify the TE concentrations and visualize and quantify the

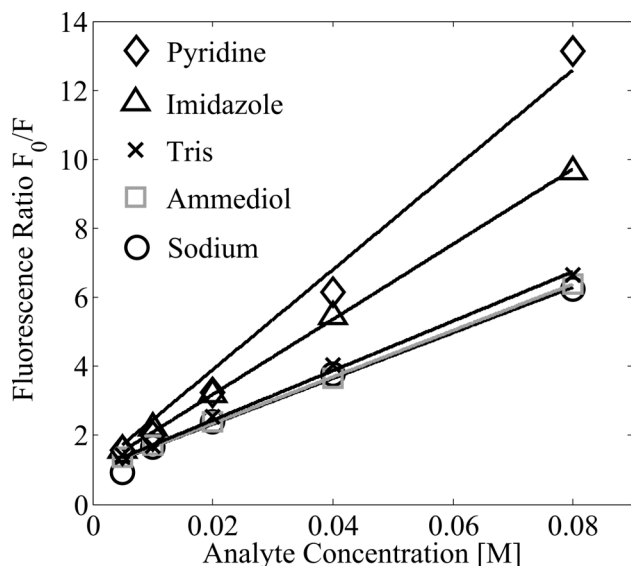


Fig. 2 Stern-Volmer plot for quenching of 6-methoxy-*N*-(3-sulfopropyl)quinolinium (SPQ) by the following buffers: pyridine-HEPES (\diamond , pH 6.2, $K_{Q,e} = 145$), imidazole-HEPES (Δ , pH 7.1, $K_{Q,e} = 109$), Tris-HEPES (\times , pH 7.3, $K_{Q,e} = 72$), ammediol-HEPES (\square , pH 7.4, $K_{Q,e} = 67$), and sodium-HEPES (\circ , pH 7.4, $K_{Q,e} = 66$). The regression coefficients R^2 are greater than 0.99 for analyte (cationic buffer component) concentrations from 5 to 80 mM, demonstrating the potential for highly accurate and selective quantitation of specific ions using SAFI.

spatiotemporal progress of cationic ITP with above described buffers.

We note we found that, for these same buffer species, the dye SAB does not follow the Stern-Volmer equation, highlighting the importance of the initial calibration in a SAFI visualization. SAB instead exhibited fluorescence enhancement by the buffers. Fluorescence enhancement has traditionally been used for detection of transition metal cations,⁴³ nucleic acids,²⁶ and various organic compounds, including saccharides.⁴⁴ The mechanisms of fluorescence enhancement vary greatly among fluorophore-enhancer pairs. For example, for acridine and ethidium dyes, fluorescence enhancement results from the screening of the fluorophore once the dye is intercalated into the nucleic acid. The screening prevents the solvent from quenching the fluorophore, resulting in the observed fluorescence enhancement.²⁶ For transition metal cation and saccharide probes, the analytes interact with the dye to increase the dye quantum yield.^{43,44} While we do not know the mechanism of fluorescence enhancement for pyridine-HEPES, imidazole-HEPES, Tris-HEPES, ammediol-HEPES, and sodium-HEPES buffers with SAB, we plot fluorescence of SAB for 5 to 80 mM base concentration for these buffers in ESI† Fig. S2. Here, we will leverage fluorescence enhancement of SAB to quantify the spatiotemporal progress of cationic ITP with our buffers, providing an interesting comparison case for the more easily calibrated SPQ visualizations.

In Fig. 3 we summarize cationic ITP experiments where SPQ and SAB were used to visualize and quantify spatiotemporal

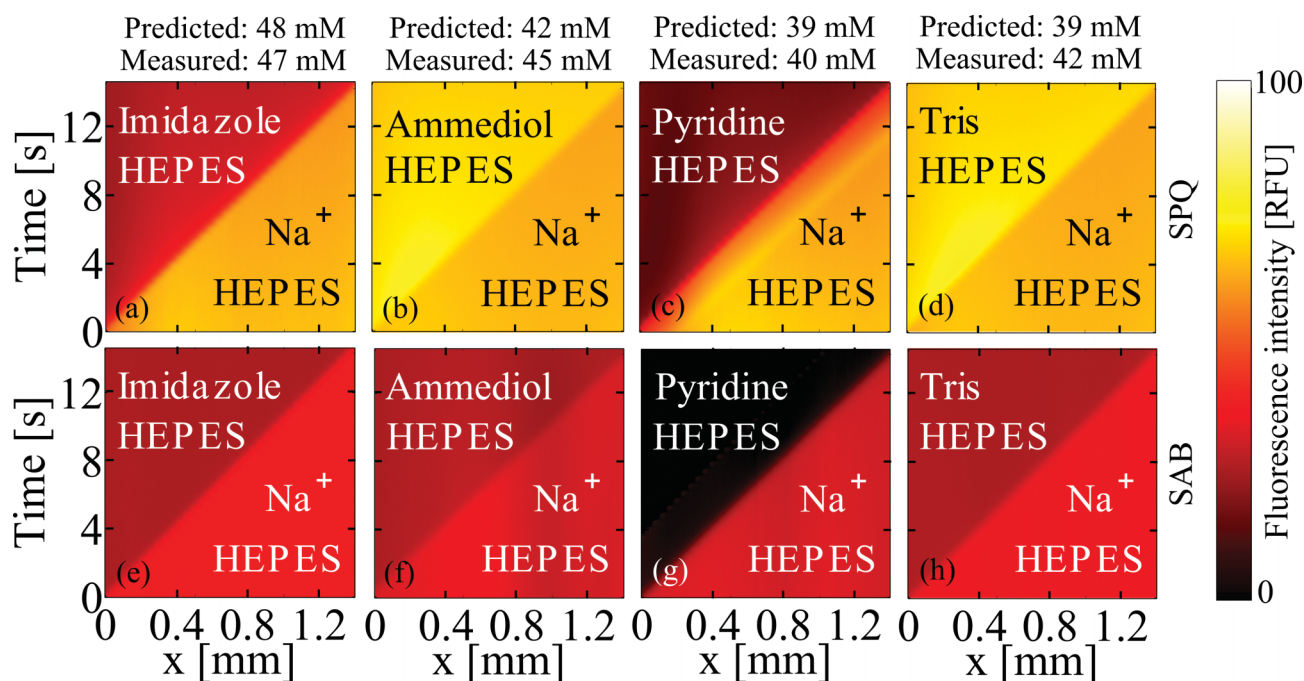


Fig. 3 Spatiotemporal plots of eight cationic isotachopheresis (ITP) experiments visualized and quantified with SPQ (a–d) and visualized with 10-(3-sulfopropyl)acridinium betaine (SAB) (e–h) (both 2.5 mM). Each spatiotemporal data plot shows measured, cross-sectional-area-averaged intensity in the microchannel of dye fluorescence vs. distance along the channel (horizontal axis, 1.4 mm) and time (vertical axis, 14.6 s). The top left region of each plot quantifies the trailing electrolyte (TE) development and the bottom right region the leading electrolyte (LE). Each dye is able to clearly visualize the interface between LE and TE and to quantify each of the analyte concentrations of interest (imidazole, ammediol, pyridine, or Tris) and interface speeds.

development of four cationic ITP processes. We plot the cross-sectional-area-averaged intensity of SAFI dye fluorescence in the channel *versus* distance along the channel, x , and time. 50 mM sodium-HEPES (pH 7.4) buffer served as the LE in all experiments, while the TE was either pyridine-HEPES (pH 6.2), imidazole-HEPES (pH 7.1), Tris-HEPES (pH 7.3) or ammediol-HEPES (pH 7.4). 1% PVP was added to both electrolytes to suppress electroosmotic flow (EOF). The experiments were performed at a constant current density of 600 A m^{-2} . SPQ and SAB are net electroneutral between pH 0–12 and therefore did not interfere with ITP.

The uniformity of fluorescence intensity within each of the moving ion zones in Fig. 3 implies uniform ion concentration density within a zone, as expected for ITP.^{14,30} The measured average interface ion concentration shock speed with both SPQ and SAB (0.1 mm s^{-1}) closely matched that predicted by the classical model of ITP (0.09 mm s^{-1}) which neglects EOF and pressure driven flow.¹⁴ In our glass microfluidic chips, EOF is in the direction of cation travel, and so it adds to the velocity of the ion concentration shock in cationic ITP. Thus we attribute the difference between predicted and measured shock speed to the presence of residual EOF in experiments. This observed interface velocity was very reproducible from experiment to experiment, deviating no more than 5% from the mean for all experiments.

We measured the concentration of the TE zone by measuring the ratio of SPQ fluorescence between the LE and TE zones and employing eqn (4) (Case 2). As with typical ITP experiments, the composition of the LE is here a known value established at the beginning of the experiment, and so the LE zone provides a convenient reference concentration for eqn (4). We measured the total concentration of imidazole, ammediol, pyridine, and Tris in the TE buffers to be 47, 45,

40, and 42 mM, respectively. We used SPRESSO³⁶ simulation to predict these concentrations as 48, 42, 39 and 39 mM respectively. Thus the measured concentrations quantified *via* SAFI agree to within less than 10% with the predicted concentrations. Each dye clearly visualizes interfaces between individual ion zones and quantifies background ion densities in these highly unsteady, non-uniform flows with high electric field gradients. We attribute the slight discrepancies between measured and predicted concentrations mainly to uncertainties in buffer contents and slight drifts in illumination intensity during quenching constant measurements.

4.2 Simultaneous visualization of multiple analyte zones in anionic ITP

We visualized two anionic ITP experiments with SPQ and SAB to demonstrate visualization of multiple analyte zones using SAFI dyes. In Fig. 4a we show the spatiotemporal development of five zones in anionic ITP visualized with 5 mM SPQ: 20 mM chloride (LE), 20 mM nitrite, 16 mM carbonic acid, 13 mM 3,5-dinitrobenzoic acid, and 12 mM HEPES (TE). Tris served as the counterion in all zones. This experiment was performed at a constant current density of 600 A m^{-2} . The predicted shock speed (0.24 mm s^{-1}) approximately matched with the measured shock speed of 0.21 mm s^{-1} . In our glass microfluidic chips, EOF is in the direction opposite of anion travel, and so it makes the apparent velocity less than that predicted by our simple ITP model which neglects EOF.

We measured the concentration of each zone behind the leading zone by measuring the ratio of fluorescence of SPQ between the leading zone (known reference concentration) and zone of interest and employing eqn (4). We measured the total base concentration of the nitrite, carbonic acid, 3,5-dinitrobenzoic acid, and HEPES to be 13, 8, 5, and 13 mM

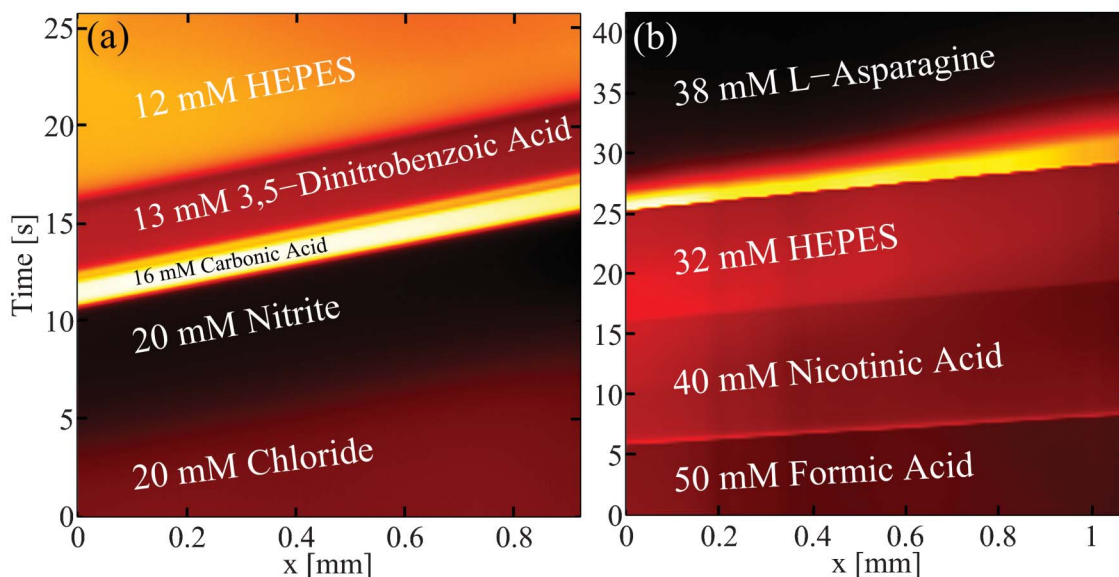


Fig. 4 Spatiotemporal plots from SAFI showing development of five ion zones migrating under anionic ITP. Here we use (a) SPQ (5 mM) and (b) SAB (2 mM) SAFI dyes. In (a) SAFI visualizes the spatiotemporal development of five distinct anion zones: chloride (LE), nitrite, carbonic acid, 3,5-dinitrobenzoic acid, and HEPES (TE). The blurred interface between the chloride and nitrite zones likely indicates zone mixing. In (b) SAFI visualizes the spatiotemporal development of formic acid (LE), nicotinic acid, HEPES, and L-asparagine (TE) zones. The bright zone observed between HEPES and L-asparagine is likely an impurity.

respectively. We used SPRESSO³⁶ simulation to predict these concentrations as 20, 16, 13 and 12 mM respectively. These results highlight the importance of calibrating dyes using precisely the same ion solutions as those expected in the experiment. We attribute most of this discrepancy to the uncertainty in the quenching constants. We also suspect this experiment may have suffered from the effects of zone sharing⁴⁵ with migrating carbonic acid. Here, the quenching constant for HEPES was obtained with solutions where the ratio of species concentrations in the calibration solution and the quantification experiment were closely matched. Thus the assumption that the ratio of species concentrations in the calibration solution is the same as in the quantification experiment (on which eqn (4) is based) was valid. Therefore, the measured HEPES concentration agreed to within better than 10% of the predicted value. However, the quenching constants for nitrite, carbonic, and 3,5-dinitrobenzoic acid were each obtained with solutions where both Tris and sodium served as the counter-ion, and this is different than the case of the experiment. Consequently, the assumption that the calibration occurred with the ratios expected in the experiment and leading to eqn (4) is not valid. Consequently, these analytes, measured concentration of anions in each zone, agreed only within 60% with the concentrations predicted by the SPRESSO simulation.³⁶ Thus, when the assumption of matching concentration ratios is relaxed, one can only obtain a rough estimate of the concentrations using eqn (4). We note that for the cases of nitrite, carbonic acid, 3,5-dinitrobenzoic acid, it is very difficult to perform calibrations using binary solutions with Tris as the sole counterion as stock supplies of these chemicals included sodium as the counter ion.

We were also able to observe using SAFI some intricate details of ITP development, such as zone mixing. For example, in Fig. 4a we observe a blurred interface between the chloride (LE) and the nitrite zone. This blurring likely indicates zone mixing which is a result of mobilities of chloride and nitrite being near each other and is consistent with our simulations.

Fig. 4a also illustrates the utility of SAFI dyes for qualitative (and in some cases quantitative) zone visualization in ITP. Traditionally ITP zones are identified by step changes in physicochemical properties such as conductivity or pH. This is because, for ITP experiments, physicochemical properties such as concentration, conductivity and pH usually vary monotonically from LE to TE.¹⁴ The minimum step change of these physicochemical properties places a limitation on the number of zones which can be resolved and on the ion mobilities which can be resolved. For such difficult-to-resolve cases, SAFI visualization (*e.g.*, using SAFI as in Fig. 4a) may enable increased resolution of ITP zones due to the non-monotonic nature of the quenching physics and its *ad hoc* dependence on quenching species. Note the high resolution of zones and highly non-monotonic values of fluorescence of zones from LE to TE in Fig. 4a.

In Fig. 4b we show the spatiotemporal development of four zones in anionic ITP visualized with 2 mM SAB: 50 mM formic acid (LE), 40 mM nicotinic acid, 32 mM HEPES, and 38 mM L-asparagine (TE). Tris served as the counterion in all zones. This experiment was performed at a constant current density of 1800 A m⁻². The predicted shock speed (0.26 mm s⁻¹)

agreed well with the measured shock speed of 0.25 mm s⁻¹. We again attribute the difference between predicted and measured shock speed to residual EOF. The zone observed between HEPES and L-asparagine is likely an impurity. Again, SAFI dye SAB clearly demarks individual ion zones in these highly unsteady, non-uniform flows with high gradients.

4.3 Visualization and quantitation of unsteady chaotic flow in EKI

We also demonstrated SAFI visualization using SPQ to visualize the unsteady, chaotic flow of a convective EKI process. The EKI setup is similar to the setup described by Posner *et al.*^{41,42} We use electroosmotic flow to focus a center, high conductivity stream between two sheath flows injected at a cross-shaped intersection as shown schematically in Fig. 1c. This sheath flow configuration is often used in flow focusing and for electrokinetic injection for on-chip-capillary electrophoresis.⁴¹ Posner and Santiago⁴¹ and Posner *et al.*⁴² present a detailed experimental study of the instability physics and chaotic dynamics of these flows. The latter studies visualized the flow by dyeing the center stream with the electroneutral fluorescent dye rhodamine B (see Table 2) and observed its fluorescence as it progressed downstream.⁴¹ This allowed for visualization of flow physics and quantitation of the motion of material lines, but did not allow for quantitation of ion concentration fields.

Here, we performed SAFI visualization by seeding a uniform concentration of SPQ in the entire flow field. This enabled us to quantify the concentration of ions in the entire flow field (both center and sheath streams). To generate the EKI flow, we drove low conductivity potassium chloride solution streams (measured conductivity of 60 $\mu\text{S cm}^{-1}$, with 10 mM HEPES and 300 $\mu\text{M KCl}$) from north and south channels. These mixed with a high conductivity potassium chloride center (east–west) stream (calculated conductivity: 3.6 S m⁻¹ calculated, 10 mM HEPES, 300 mM KCl). Since the concentration of HEPES remains invariant in the entire flow field, while the concentration of potassium chloride is diluted, we may use Case 3 described in Section 2 of the ESI† to quantify the concentration of potassium chloride in the entire flow field.

To generate the EKI flow, we drove low conductivity potassium chloride solutions from north and south channels, which mixed with a high conductivity potassium chloride center stream with order 450 V cm⁻¹ electric field (see Fig. 1c). In Fig. 5 we show two dimensional, full-field visualizations of this convective electrokinetic instability at five times, each 10 ms apart using 4 mM SPQ. These images highlight the unsteady, fully-chaotic nature of this flow. SPQ fluorescence captured both the transverse velocity fluctuations of the secondary flow and can be used to quantitatively measure local ion densities as the EKI mixes the center stream with two sheath streams. As an example, we used these data to determine the characteristic temporal frequency of oscillation of the center stream. We extracted fluorescence intensity of a small region from the set of 377 images taken at 100 frames per second. This region is indicated by a small square in the first frame of Fig. 5a. We performed a discrete Fourier transform on this data and obtained the frequency power spectrum shown in Fig. 5b, which shows a strong 25 Hz

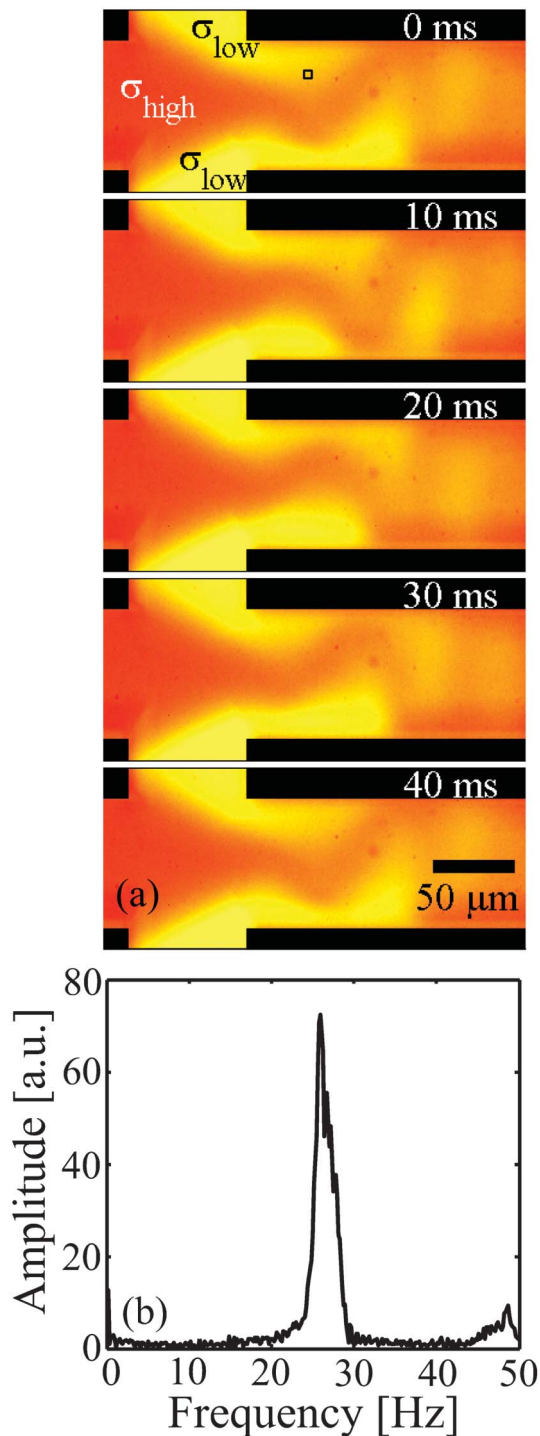


Fig. 5 (a) Two dimensional, full-field visualization of a convective electrokinetic instability (EKI) at five times using SAFI (using SPQ at 4 mM). Low conductivity streams (yellow, (white in BW), $60 \mu\text{S cm}^{-1}$, 10 mM HEPES, 300 μM KCl) from top and bottom were mixed with a high conductivity center stream (red (or gray in BW), 3.6 S m^{-1} , 10 mM HEPES, 300 mM KCl) and driven by order 450 V cm^{-1} electric field. This configuration is well known to result in EKI at high fields.⁴¹ SAFI is able to simultaneously visualize material lines between the two streams and quantify the dynamics of potassium chloride concentration in the entire field. (b) Discrete Fourier transform of intensity of the average of points in the square in the first frame of (a) (acting as a virtual point detector). The data is taken at 100 frames per second for 3.8 s. The frequency of center stream oscillation is around 25 Hz.

oscillation for this flow. This value agrees with the frequencies observed by Posner and Santiago⁴¹ at similar conditions.

4.4 Limitations of method

The main limitations of SAFI quantitation are the availability of suitable dyes for analytes of interest, the number of calibration experiments needed to quantify complicated mixtures, and identifying and dealing with unexpected dye-quencher interactions. When quantifying analyte concentrations in complicated mixtures a significant number of dyes may be needed (see Section 2.2. above). Furthermore, for complicated mixtures, a large number of calibration experiments may also be needed. The latter limitation may be mitigated somewhat by using automated pipetting systems or employment of simple microfluidic metering chips⁴⁶ to prepare calibration solutions. Lastly, for some analytes it may be difficult to find a dye which is appreciably quenched by the analyte.

5. Conclusions and future work

We demonstrated a novel method for full-field 2D scalar visualization and quantification of species concentration fields that we termed species-altered fluorescence imaging (SAFI). This method employs electrically neutral, non-interfering fluorescent dyes whose quantum yields are selectively quenched or enhanced by analyte species. We described criteria for choosing SAFI dyes and tabulated 35 promising SAFI dyes and their excitation and emission wavelengths, aqueous solubility, quenching constants and other properties. Further, we described species concentration field quantification *via* Stern-Volmer quenching and discussed method sensitivity and resolution. Next we experimentally demonstrated our method with two SAFI dyes: 6-methoxy-*N*-(3-sulfopropyl)quinolinium (SPQ) and 10-(3-sulfopropyl)acridinium betaine (SAB). We demonstrated our method in full-field spatiotemporal visualization and quantitation of isotachopheresis (ITP) in both cationic and anionic modes and in a convective electrokinetic instability (EKI) flow. In cationic ITP we quantified the development and concentration of the trailing zone and measured the ion concentration shock velocity with four trailing zones and two SAFI dyes. The measured concentrations agreed within better than 10% with those predicted and measured shock velocities within better than 5% of the mean shock velocity. In anionic ITP we simultaneously quantified the development and concentration of up to five analyte zones. Here SAFI was also able to accurately measure shock velocities and additionally visualize flow nuances such as zone mixing and zones due to impurities. In EKI we quantified a highly unsteady, fully-chaotic flow instability sometimes encountered in electrokinetic flow focusing. SAFI captured both the transverse velocity fluctuations of the secondary flow and quantitatively measured local ion densities as the EKI mixes the center stream with two sheath streams. In these experiments SAFI clearly visualized interfaces between ion zones and material

interfaces, and accurately quantified local ion concentrations in these highly unsteady and non-uniform flows with high gradients. Throughout these discussions, we also described several visualizations and calibrations which highlight the importance of careful calibration of a chosen SAFI dye.

Possible significant extensions of the current work include SAFI visualization employing simultaneously multiple dyes in same solution. Also of interest would be the application of SAFI to study reacting electrokinetic flows, such as those near electrodes. Of further possible interest is the application of SAFI to visualize ion density fields in non-aqueous solvents and solvent mixtures.

Acknowledgements

We gratefully acknowledge support from the National Science Foundation for a Graduate Research Fellowship for Viktor Shkolnikov. We also gratefully acknowledge support from Defense Advanced Research Projects Agency under contract No. HR0011-12-C-0080, program manager Daniel J. Wattendorf. We also gratefully acknowledge support from the National Science Foundation under contract No. CBET-1159092.

References

- 1 A. E. Kamholz, *Lab Chip*, 2004, **4**, 16N–20N.
- 2 D. Mark, S. Haeberle, G. Roth, F. von Stetten and R. Zengerle, *Chem. Soc. Rev.*, 2010, **39**, 1153–1182.
- 3 D. Sinton, *Microfluid. Nanofluid.*, 2004, **1**, 2–21.
- 4 *Microscale Diagnostic Techniques*, ed. K. Breuer, Springer, 2005.
- 5 P. H. Paul, M. G. Garguilo and D. J. Rakestraw, *Anal. Chem.*, 1998, **70**, 2459–2467.
- 6 B. M. Mosier, J. M. Molho and J. S. Santiago, *Exp. Fluids*, 2002, **33**, 545–554.
- 7 H. Y. Park, X. Qiu, E. Rhoades, J. Korlach, L. W. Kwok, W. R. Zipfel, W. W. Webb and L. Pollack, *Anal. Chem.*, 2006, **78**, 4465–4473.
- 8 J. B. Knight, A. Vishwanath, J. P. Brody and R. H. Austin, *Phys. Rev. Lett.*, 1998, **80**, 3863–3866.
- 9 D. E. Hertzog, B. Ivorra, B. Mohammadi, O. Bakajin and J. G. Santiago, *Anal. Chem.*, 2006, **78**, 4299–4306.
- 10 *Handbook of Capillary Electrophoresis*, ed. J. P. Landers, CRC Press, Boca Raton, FL, 1994.
- 11 M. S. Munson, C. R. Cabrera and P. Yager, *Electrophoresis*, 2002, **23**, 2642–2652.
- 12 J. C. Reijenga, T. P. E. M. Verheggen and F. M. Everaerts, *J. Chromatogr., A*, 1984, **283**, 99–111.
- 13 R. D. Chambers and J. G. Santiago, *Anal. Chem.*, 2009, **81**, 3022–3028.
- 14 F. M. Everaerts, J. L. Beckers and T. P. E. M. Verheggen, *Isotachophoresis: Theory, Instrumentation, and Applications*, Elsevier, Amsterdam, New York, 1976.
- 15 A. T. Woolley, K. Lao, A. N. Glazer and R. A. Mathies, *Anal. Chem.*, 1998, **70**, 684–688.
- 16 K. Swinney and D. J. Bornhop, *Electrophoresis*, 2000, **21**, 1239–1250.
- 17 A. S. Verkman, *Am. J. Physiol. Cell Physiol.*, 1990, **259**, C375–C388.
- 18 C. D. Geddes, *Meas. Sci. Technol.*, 2001, **12**, R53.
- 19 Invitrogen, 6-methoxy-N-(3-sulfopropyl)quinolinium, inner salt (SPQ), <http://products.invitrogen.com/ivgn/product/M440>.
- 20 Sigma-Aldrich, 10-(3-sulfopropyl)acridinium betaine <http://www.sigmaaldrich.com/catalog/product/fluka/86181?lang=en®ion=US>.
- 21 R. Krapf, N. P. Illsley, H. C. Tseng and A. S. Verkman, *Anal. Biochem.*, 1988, **169**, 142–150.
- 22 ACD/Labs, V11.02 edn, 2012.
- 23 C. Huber, K. Fährlich, C. Krause and T. Werner, *J. Photochem. Photobiol., A*, 1999, **128**, 111–120.
- 24 N. O. McHedlov-Petrosyan, V. I. Kukhtik and V. I. Alekseeva, *Dyes Pigm.*, 1994, **24**, 11–35.
- 25 J. R. Lakowicz, *Principles of Fluorescence Spectroscopy*, Springer, New York, 2006.
- 26 A. P. Demchenko, *Introduction to Fluorescence Sensing*, Springer, Kiev.
- 27 B. Valeur, *Molecular Fluorescence: Principles and Applications*, Wiley-VCH Verlag GmbH, Weinheim, 2001.
- 28 G. Strang, *Linear Algebra and Its Applications*, Thomson, 2006.
- 29 V. Shkolnikov, S. S. Bahga and J. G. Santiago, *Phys. Chem. Chem. Phys.*, 2012, **14**, 11534–11545.
- 30 G. Garcia-Schwarz, A. Rogacs, S. S. Bahga and J. G. Santiago, *JoVE*, 2012, e3890.
- 31 P. Bocek, *Analytical Isotachophoresis*, VCH, Weinheim, Cambridge, 1987.
- 32 S. S. Bahga, M. Bercovici and J. G. Santiago, *Electrophoresis*, 2010, **31**, 910–919.
- 33 G. V. Kaigala, M. Bercovici, M. Behnam, D. Elliott, J. G. Santiago and C. J. Backhouse, *Lab Chip*, 2010, **10**, 2242–2250.
- 34 S. S. Bahga, R. D. Chambers and J. G. Santiago, *Anal. Chem.*, 2011, **83**, 6154–6162.
- 35 S. S. Bahga and J. G. Santiago, *Electrophoresis*, 2012, **33**, 1048–1059.
- 36 M. Bercovici, S. K. Lele and J. G. Santiago, *J. Chromatogr., A*, 2009, **1216**, 1008–1018.
- 37 S. S. Bahga, M. Bercovici and J. G. Santiago, *Electrophoresis*, 2012, **33**, 3036–3051.
- 38 H. Lin, B. D. Storey, M. H. Oddy, C. H. Chen and J. G. Santiago, *Phys. Fluids*, 2004, **16**, 1922–1935.
- 39 C.-H. Chen, H. Lin, S. K. Lele and J. G. Santiago, *J. Fluid Mech.*, 2005, **524**, 263–303.
- 40 A. Persat and J. G. Santiago, *New J. Phys.*, 2009, **11**, 075026.
- 41 J. D. Posner and J. G. Santiago, *J. Fluid Mech.*, 2006, **555**, 1–42.
- 42 J. D. Posner, C. L. Pérez and J. G. Santiago, *Proc. Natl. Acad. Sci. U. S. A.*, 2012, **109**, 14353–14356.
- 43 K. Rurack, *Spectrochim. Acta, Part A*, 2001, **57**, 2161–2195.
- 44 H. Cao and M. D. Heagy, *J. Fluoresc.*, 2004, **14**, 569–584.
- 45 T. K. Khurana and J. G. Santiago, *Lab Chip*, 2009, **9**, 1377–1384.
- 46 C. L. Hansen, E. Skordalakes, J. M. Berger and S. R. Quake, *Proc. Natl. Acad. Sci. U. S. A.*, 2002, **99**, 16531–16536.